Scientific Research Publishing

Open Journal of Antennas and Propagation, 2023, 11, 1-10
https://www.scirp.org/journal/ojapr
ISSN Online: 2329-8413
ISSN Print: 2329-8421

Miniaturized Electronically Steerable Parasitic Array Antenna

Shafaq Kausar[1], Ahmed Kausar[2], Hani Mehrpouyan[1], Muhammad Hadi[3], Salahuddin Tariq[4]

[1]Department of Electrical and Computer Engineering, Boise State University, Boise, ID, USA
[2]Arts & Science Division at University of Toronto, Toronto, Canada
[3]School of Engineering, Ulster University, Belfast, United Kingdom
[4]Department of Electrical and Computer Engineering, University of Texas at Dallas, Richardson, TX, USA
Email: shafaq.omar@yahoo.com

How to cite this paper: Kausar, S., Kausar, A., Mehrpouyan, H., Hadi, M. and Tariq, S. (2023) Miniaturized Electronically Steerable Parasitic Array Antenna. *Open Journal of Antennas and Propagation*, **11**, 1-10.
https://doi.org/10.4236/ojapr.2023.111001

Received: August 29, 2022
Accepted: March 13, 2023
Published: March 16, 2023

Abstract

In this article we propose a miniaturized dual-band electronically steerable parasitic array radiator (ESPAR) antenna. The antenna can generate up to two steerable beams. The beam-steering range of the proposed antenna is 360˚ in the azimuth plane. The antenna's eual-band coverage includes the frequency ranges from 2.3 GHz to 2.53 GHz and from 2.9 GHz to 3.7 GHz. The antenna consists of six folded parasitic monopole elements surrounding an active conical element. The folded monopole element design offers three times lower antenna height than that of the conventional ESPAR antennas. The active element has conical shape and it is larger in length than the parasitic monopole elements, this enables the dual-band operation. Thus, the proposed design is not only smaller than the conventional ESPAR antennas but it also achieves dual-band operation. Despite its compact design, the antenna has a peak gain of 6.3 dBi, which is equivalent to the gain of conventional ESPAR antennas. These characteristics make the antenna a good candidate for next generation communication systems.

Keywords

5G, IoT, Antenna, Phased Array, Wifi, ESPAR, Wireless

1. Introduction

Smart antennas have capability of adaptive beam-forming. For WLAN applications the smart antennas can improve the received signal-to-interference ratio by placing a null in the direction of interference and the maxima towards the desired signal source [1]. Electronically steerable parasitic array radiator antennas

(ESPAR) provide a simple and cost effective beam steering solution. ESPAR antennas are typically not low profile and miniaturization is required for using such antennas in compact devices. In this paper, we propose a miniaturized ESPAR antenna with a broad bandwidth and a single/dual lobe radiation pattern. The design of the miniaturized seven element ESPAR antenna consists of a circular array of six parasitic elements around a central active element. Our design is three times smaller in height compared to a conventional ESPAR antenna [2] and supports single/dual lobe radiation patterns and dual band coverage.

Previously designed miniaturized/slim ESPAR antennas have resulted in lower gains [3] [4]. The proposed miniaturized ESPAR antenna is superior to miniaturized ESPAR antennas in [3] [4] in terms of gain and bandwidth. Miniaturized ESPAR antennas discussed in [3] [4] [5] [6] have limited bandwidth and support single lobe radiation pattern. The proposed design supports reconfigurable single and dual lobe radiation patterns, its dual-band coverage includes the frequency ranges 2.3 GHz - 2.53 GHz and 2.9 GHz - 3.7 GHz. Dual lobe antennas can play an important role in increasing network capacity without using additional antennas by providing beam diversity which is effective in addressing obstruction. As a result, such antennas can considerably enhance the reliability of the wireless system in non-line-of-sight links.

In the proposed model six parasitic monopoles are mounted on a skirted ground plane. The electric field of a seven element ESPAR antenna can be calculated by using the vector effective length equivalent weight vector method [7].

$$E(\theta,\phi) = -j\frac{Z_0}{2\lambda}\frac{e^{-jkr}}{r}\sum_{m=0}^{6}\ell e_m(\theta) i_m a_m(\theta,\phi) \tag{1}$$

where Z_0 is the characteristic impedance, a_m is the steering vector that is expressed as [7]:

$$a_m(\theta,\phi) = exp^{jk(\sin\theta\cos\phi x_m + \sin\theta\sin\phi y_m + \cos\theta z_m)}$$

le_m is the vector effective length and is expressed as:

$$le_m = le_m^0(1-\alpha_m x_m) \tag{2}$$

i_m is the port current that is expressed as:

$$\begin{bmatrix} i_0 \\ i_1 \\ i_2 \\ i_3 \\ i_4 \\ i_5 \\ i_6 \end{bmatrix} = \left(\left[Z_{mn}\right] + diag\left[Z_x, jX_1, jX_2, jX_3, \cdots, jX_6\right]\right)^{-1} \begin{bmatrix} vs \\ 0 \\ 0 \\ 0 \\ 0 \\ 0 \\ 0 \end{bmatrix} \tag{3}$$

Here, X_1, X_2, X_3, X_4, X_5 and X_6 are reactances loaded on each parasitic element. By varying these reactances the port current varies and the antenna beam is steered. Therefore, the antenna gain can be expressed as:

$$D(\theta,\phi)=\frac{\pi Z_0 \sin\theta\left|\sum_{m=0}^{M} I_m i_m\Big|_{Zs=0} a_m(\theta,\phi)\right|^2}{\lambda^2 |v_s|^2 Re\left(\frac{1}{Z_{in}}\right)} \quad (4)$$

The proposed design has a gain of 6.3 dBi, which is 2.3 dB higher than comparable size slim/miniaturized ESPAR antennas [3]. The miniaturized ESPAR antenna designed in [3] has a peak gain of 4 dBi. In comparison, the proposed design has 2.3 dB higher gain, and the antenna has the capability of single/dual beam forming along with dual band operation. The key differentiators of our design are:

- The height of the proposed design is three times lower than conventional ESPAR antennas.
- Capable of forming up to two reconfigurable beams.
- Supports dual band operation (2.3 - 2.53 GHz and 2.9 - 3.7 GHz).
- Antenna beam can be steered by a simple switching mechanism.

2. Antenna Design Overview

In typical seven element ESPAR antennas there is an array of six parasitic monopole elements around a central active element and each monopole is $\lambda/4$ in height [8] [9]. The simulated model of the designed antenna is shown in **Figure 1**. The antenna consists of a conical active element and folded monopole passive elements. The folded monopoles consist of three arms, where each arm is $\lambda/12$ in length and all three arms of the folded monopole collectively form a length of $\lambda/4$ [10]. Folded monopoles are used to reduce the antenna height. The central active element is made conical in order to improve the bandwidth, the upper radius of the central conical element is 1.4 mm and the lower radius is 1 mm. The Length of the active element is set to $\lambda/5$. It has a larger height than the surrounding parasitic monopoles, which is what allows for the dual band nature of the antenna.

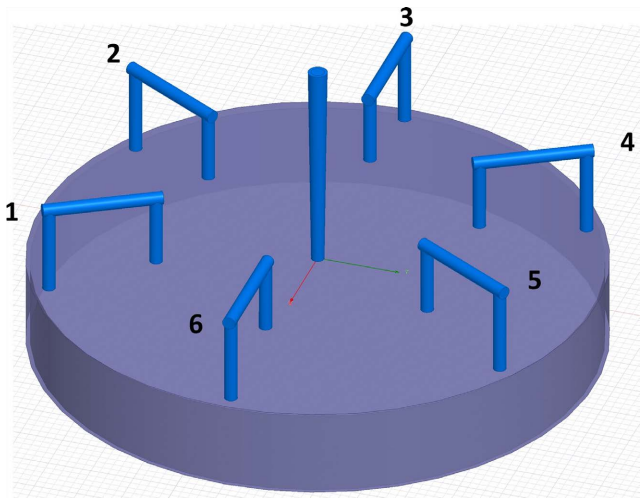

Figure 1. HFSS simulated antenna model (front view).

Table 1. Size comparison between proposed antenna and conventional ESPAR antenna.

Design Parameter	Miniaturized dual-band ESPAR	Conventional ESPAR
Folded monopole height	$\lambda/12$	$\lambda/4$
Central element length	$\lambda/5$	$\lambda/4$
Central Element geometry	Conical	Cylindrical
Ground Radius	$\lambda/4$	$\lambda/2$

The height of the ground plane is $\lambda/5$ and it is skirted. The radius of the ground plane in the proposed antenna is $\lambda/4$, whereas in conventional ESPAR antennas the radius of the ground plane is $\lambda/2$. Table 1 shows the size comparison between the proposed miniaturized dual-band ESPAR antenna and a conventional ESPAR antenna.

3. Simulated Model and Beam Forming Configuration

Monopole antennas are generally sensitive to inductive and capacitive changes. In conventional ESPAR antennas, varactors are used to produce variable capacitive effects for beam steering [9]. By varying the capacitive loading of the parasitic monopole elements, the effective length is changed and the elements tend to act as reflectors or directors. In the proposed design instead of varying the capacitive loading, we open or short the parasitic monopoles thereby achieving a similar effect in a more cost effective manner. In the high frequency structure simulator (HFSS) simulations the active element is loaded with a lumped port excitation. Further, the parasitic elements are electrically shortened by using perfect electric boundaries.

The simulated antenna model has a return loss of 15.2 dB at 2.45 GHz and 43 dB at 3.25 GHz. Figure 2 shows the return loss plot of the designed antenna. Considering S_{11} = −10 dB as our reference point antenna bandwidth, it is 220 MHz for band 1 since S_{11} is below −10 dB from 2.31 GHz to 2.53 GHz. Similarly, the antenna bandwidth is 800 MHz for band 2 as S_{11} is below −10 dB from 2.9 GHz to 3.7 GHz.

Parasitic monopoles are placed at an angle of 60˚ from each other. The element along the x-axis is denoted as element 1 and all other elements are marked counterclockwise with respect to element 1, as shown in Figure 1. The beam is formed between two open elements as open elements act as directors and short elements act as reflectors. When element 1 and 2 are open and all other elements are shorted, the beam is formed between elements 1 and 2. Similarly, when element 2 and 3 are open and the remaining elements are shorted the beam is formed between these two elements, and so on. Mechanical shorts were used for opening and shorting the parasitic elements, but these would be replaced with solid-state components in a practical implementation. The beam control switching configurations are detailed in Table 2. The antenna main beam is

steered between 0 - 360 degrees in steps of 60˚ each. Figure 3 shows 2D radiation pattern of the designed antenna at −90˚, −30˚ and +30˚ respectively. Figure 4 shows 2D radiation pattern of the designed antenna at 90˚, 150˚ and −150˚ respectively.

To achieve a single lobe radiation pattern two adjacent monopoles are to be opened, whereas to produce a dual lobe beam pattern two oppositely placed monopoles are opened. 2D single lobe patterns of the designed antenna are shown in Figure 3 and Figure 4. Dual lobe radiation patterns are shown in Figure 5.

4. Antenna Fabrication and Measurement Results

The monopoles and central elements are made from brass and the ground plane is made up of aluminum. The monopoles are mounted on a ground plane by

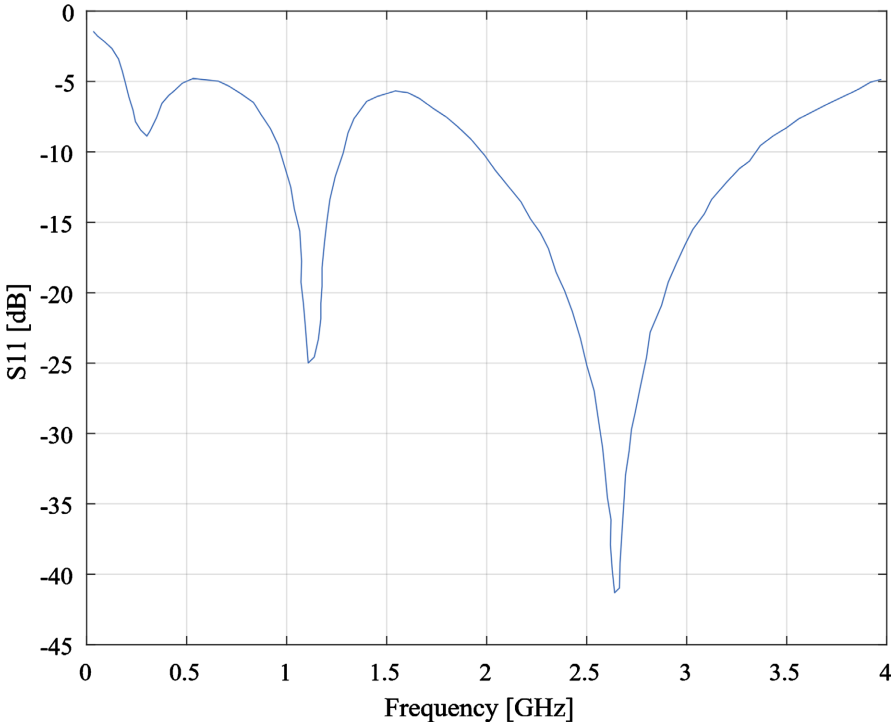

Figure 2. S_{11} plot of designed antenna.

Table 2. Beam direction and control configuration.

Angle (degrees)	Elem1	Elem2	Elem3	Elem4	Elem5	Elem6
30˚	Open	Open	Short	Short	Short	Short
90˚	Short	Open	Open	Short	Short	Short
150˚	Short	Short	Open	Open	Short	Short
210˚	Short	Short	Short	Open	Open	Short
270˚	Short	Short	Short	Short	Open	Open
330˚	Open	Short	Short	Short	Short	Open

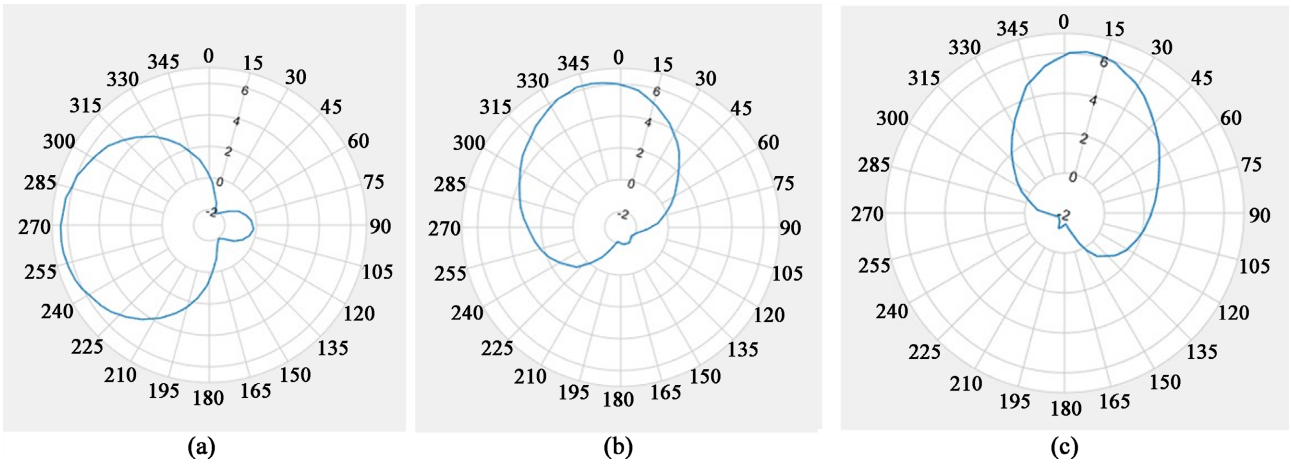

Figure 3. 2D radiation pattern (a) steered at −90˚; (b) steered at −30˚; (c) steered at 30˚.

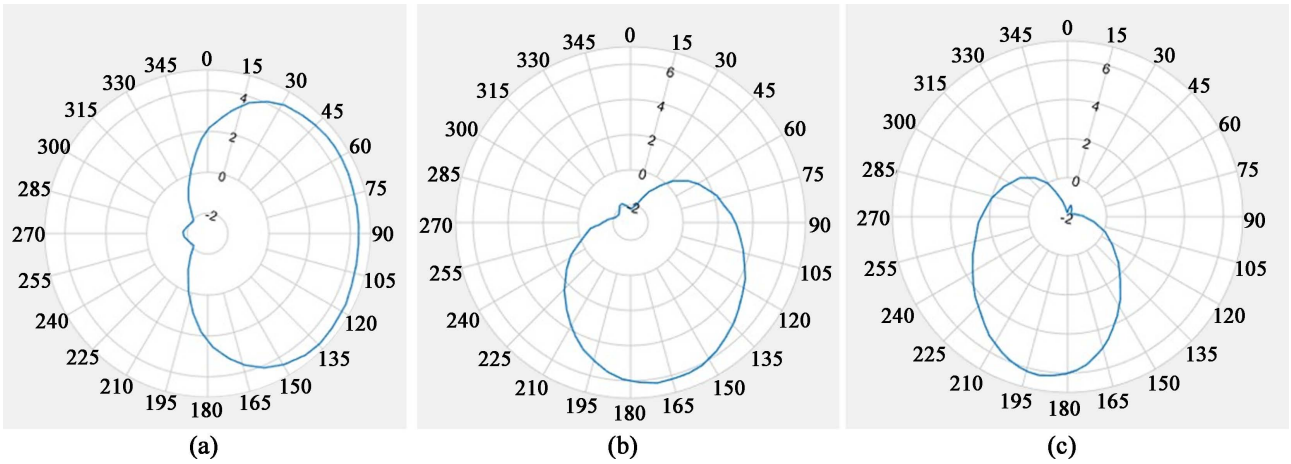

Figure 4. 2D radiation pattern (a) steered at 90˚; (b) steered at 150˚; (c) steered at −150˚.

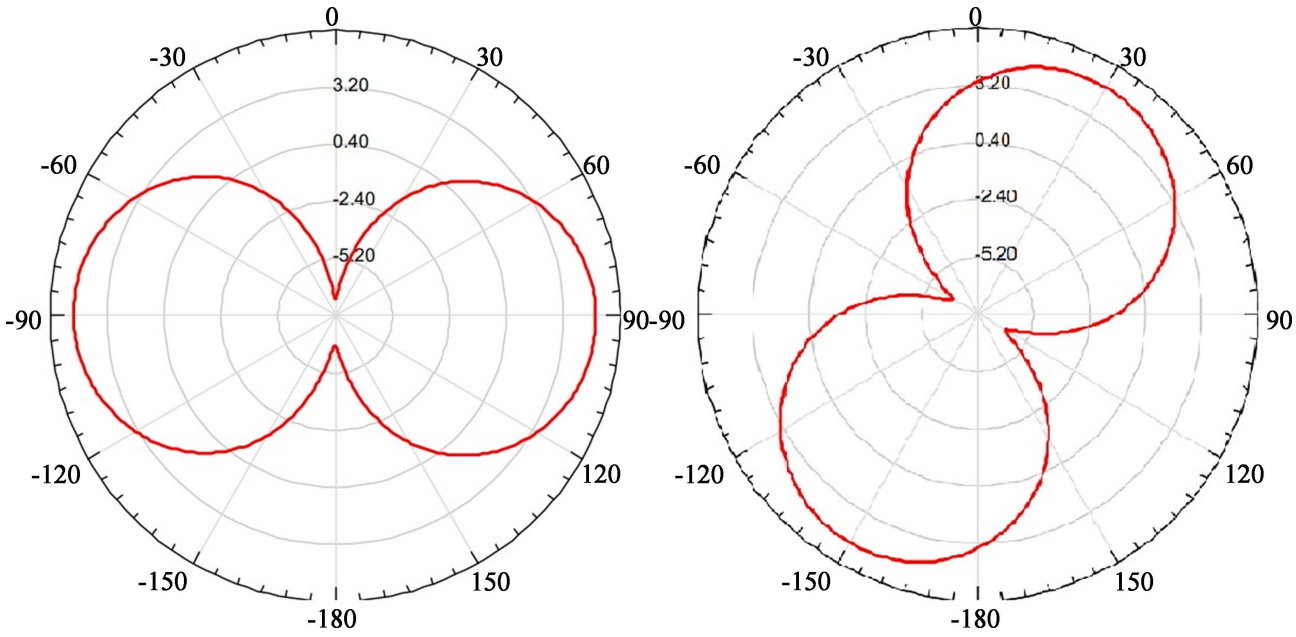

Figure 5. 2D dual lobe radiation pattern at 90˚/−90˚.

using SMA connectors. Figure 6 and Figure 7 show front view and side view of fabricated antenna. RF shorts are used for opening/shorting of the antenna monopoles for beam steering.

The designed antenna was tested in an anechoic chamber and the measured results aligned well with HFSS simulated results. However, the simulated S_{11} value was better as compared to measured one because the antenna elements were considered perfect electric conductor in the HFSS antenna simulations. Figure 8 shows S_{11} plot when element 1, 2, 3 and 4 are shortened and Figure 9 shows S_{11} plot when element 2, 3, 4 and 5 are shortened.

The radiation pattern of the designed antenna was measured in an anechoic chamber and the measured results show complete 360˚ beam steering in azimuth plane. Figure 10, and Figure 11 show the measured radiation patterns of the designed antenna at 90˚, 165˚ and 195˚, respectively. These measured results are aligned well with simulated results.

5. Conclusion

This paper presented the design of a miniaturized dual-band and dual-lobe

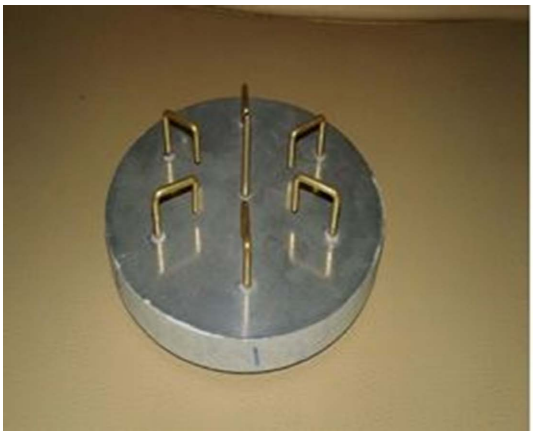

Figure 6. Fabricated antenna (front view).

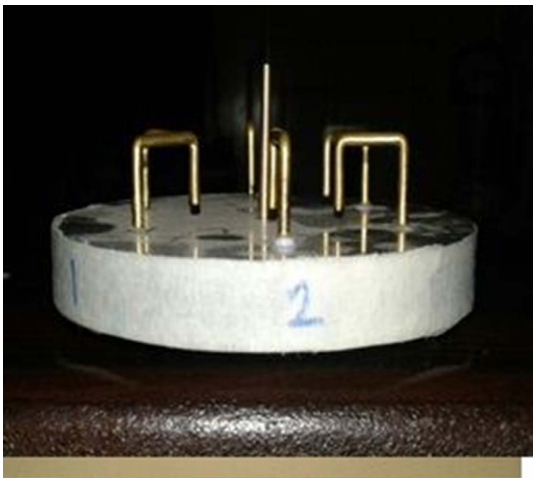

Figure 7. Fabricated antenna (side view).

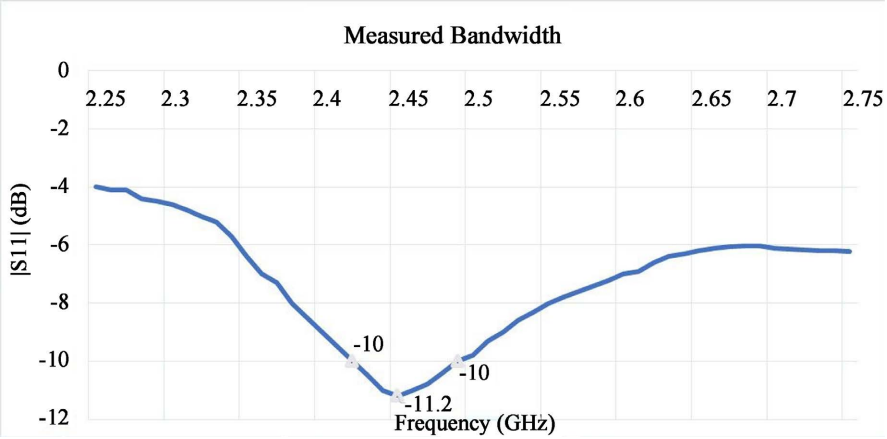

Figure 8. Measured S_{11} plot (Element 1, 2, 3 and 4 shortened).

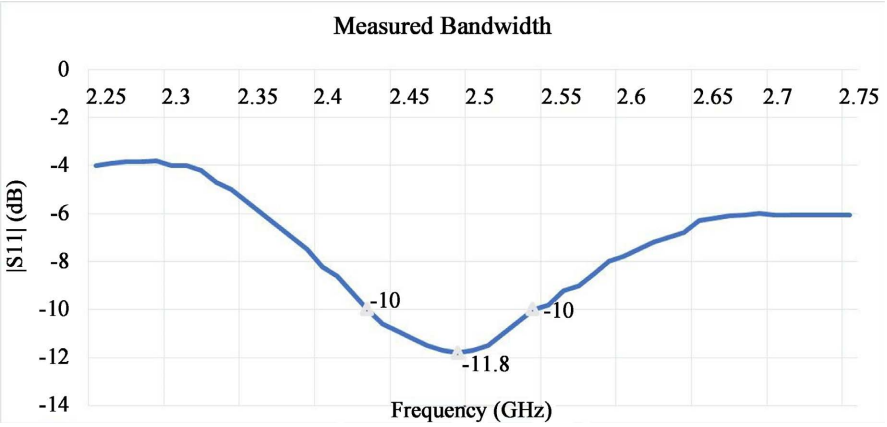

Figure 9. Measured S_{11} plot (element 2, 3, 4 and 5 shortened).

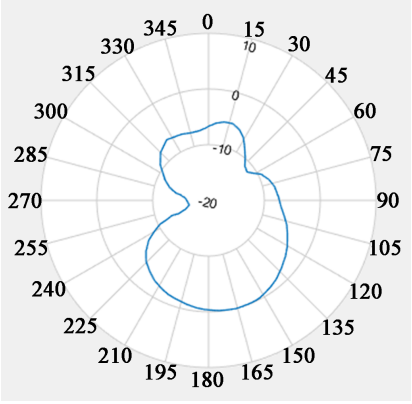

Figure 10. Measured radiation pattern steered at 160˚.

ESPAR antenna with enhanced bandwidth for WLAN applications. The height of the proposed antenna is three times lower than that of conventional ESPAR antennas. The proposed antenna offers dual bandwidth characteristics and covers the bands from 2.3 - 2.53 GHz and 2.9 GHz - 3.7 GHz. The proposed antenna is capable of replacing standard ESPAR antennas as it has a more compact structure, dual-band coverage, and both single and dual lobe radiation pattern

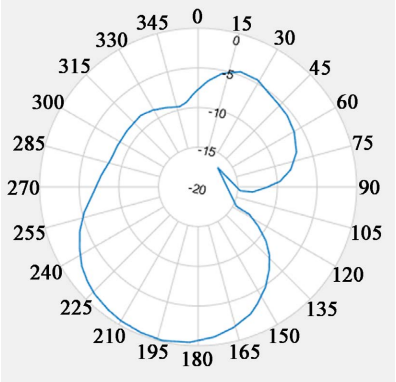

Figure 11. Measured radiation pattern steered at 200˚.

options. The switching mechanism used for beam steering is cost effective and easy to implement while allowing sufficient angular resolution in beam steering. The achieved peak gain was 6.3 dBi, and it is anticipated that similar structures can be implemented at mm-Wave frequencies. Future prospects of the proposed design include gain enhancement for applications requiring high gain. Gain can be increased by phase combining two or more circular monopole arrays.

Conflicts of Interest

The authors declare no conflicts of interest regarding the publication of this paper.

References

[1] Dai, L.L., Wang, B.C., Wang, M., Yang, X., Tan, J.B., *et al.* (2020) Reconfigurable Intelligent Surface-Based Wireless Communications: Antenna Design, Prototyping, and Experimental Results. *IEEE Access*, **8**, 45913-45923. https://doi.org/10.1109/ACCESS.2020.2977772

[2] Groth, M., Rzymowski, M., Nyka, K. and Kulas, L. (2020) ESPAR Antenna-Based WSN Node with DoA Estimation Capability. *IEEE Access*, **8**, 91435-91447. https://doi.org/10.1109/ACCESS.2020.2994364

[3] Liu, H.T., Gao, S. and Loh, T.H. (2012) Electrically Small and Low Cost Smart Antenna for Wireless Communication. *IEEE Transactions on Antennas and Propagation*, **60**, 1540-1549. https://doi.org/10.1109/TAP.2011.2180300

[4] Zhang, L., Gao, S., Luo, Q., Young, P.R. and Li, Q.X. (2016) Planar Ultrathin Small Beam-Switching Antenna. *IEEE Transactions on Antennas and Propagation*, **64**, 5054-5063. https://doi.org/10.1109/TAP.2016.2620490

[5] Iigusa, K., Sato, K. and Fujise, M. (2006) A Slim Electronically Steerable Parasitic Array Radiator Antenna. 2006 6*th International Conference on ITS Telecommunications*, Chengdu, 21-23 June 2006, 386-389. https://doi.org/10.1109/ITST.2006.288922

[6] Liu, H., Gao, S. and Loh, T. (2013) Small Director Array for Low-Profile Smart Antennas Achieving Higher Gain. *IEEE Transactions on Antennas and Propagation*, **61**, 162-168. https://doi.org/10.1109/TAP.2012.2219841

[7] Iigusa, K. and Ohira, T. (2004) A Simple and Accurate Mathematical Model of Electronically Steerable Parasitic Array Radiator Antennas. *First IEEE Consumer*

Communications and Networking Conference 2004, Las Vegas, 5-8 January 2004, 312-315.

[8] Abdullah, N. and Kuwahara, Y. (2010) A Study of ESPAR Antenna. 2010 *International Conference on Microwave and Millimeter Wave Technology*, Chengdu, 8-11 May 2010, 1999-2002. https://doi.org/10.1109/ICMMT.2010.5525159

[9] Lu, J., Ireland, D. and Schlub, R. (2004) Development of ESPAR Antenna Array Using Numerical Modelling Techniques. *Proceedings. ICCEA* 2004. 2004 3*rd International Conference on Computational Electromagnetics and Its Applications,* 2004, Beijing, 1-4 November 2004, 182-185.

[10] Tarkowski, M. and Kulas, L. (2019) RSS-Based DoA Estimation for ESPAR Antennas Using Support Vector Machine. *IEEE Antennas and Wireless Propagation Letters*, **18**, 561-565. https://doi.org/10.1109/LAWP.2019.2891021